Fluorescence intensity and bright spot analyses using a confocal microscope for photodynamic diagnosis of brain tumors

Fluorescence intensity and bright spot analyses using a confocal microscope for photodynamic diagnosis of brain tumors

Takeshi Yoneyama[a,*], Tetsuyo Watanabe[a], Hiroyuki Kagawa[a], Yutaka Hayashi[b], Mitsutoshi Nakada[b]

[a] *School of Mechanical Engineering, Kanazawa University, Kakuma-machi, Kanazawa 920-1192, Japan*

[b] *Department of Neurosurgery Graduate School of Medical Science, Kanazawa University*

Takara-machi, Kanazawa 920-8641, Japan

*Corresponding author. yoneyama@se.kanazawa-u.ac.jp

Abstract

Background: In photodynamic diagnosis using 5-aminolevulinic acid (5-ALA), discrimination between the tumor and normal tissue is very important for a precise resection. However, it is difficult to distinguish between infiltrating tumor and normal regions in the boundary area. In this study, fluorescent intensity and bright spot analyses using a confocal microscope is proposed for the precise discrimination between infiltrating tumor and normal regions.

Methods: From the 5-ALA-resected brain tumor tissue, the red fluorescent and marginal regions were sliced for observation under a confocal microscope. Hematoxylin and eosin (H&E) staining was performed on serial slices of the same tissue. According to the pathological inspection of the H&E slides, the tumor and infiltrating and normal regions on confocal microscopy images were investigated. From the fluorescent intensity of the image pixels, a histogram of pixel number with the same fluorescent intensity was obtained. The fluorescent bright spot sizes and total number were compared between the marginal and normal regions.

Results: The fluorescence intensity distribution and average intensity in the tumor were different from those in the normal region. The probability of a difference from the dark enhanced the difference between the tumor and the normal region. The bright spot size and number in the infiltrating tumor were different from those in the normal region.

Conclusions: Fluorescence intensity analysis is useful to distinguish a tumor region, and a bright spot analysis is useful to distinguish between infiltrating tumor and normal regions. These methods will be important for the precise resection or photodynamic therapy of brain tumors.

Key words

Neurosurgery, photodynamic diagnosis, brain tumor, fluorescence intensity, confocal microscope

1. Introduction

A precise resection of a glioblastoma (GBM) affects the postoperative survival time of patients. On the other hand, an excessive resection around the tumor may cause brain damage. It is crucial to differentiate between the tumor region to be removed and the normal region that should not be removed.

Photodynamic diagnosis (PDD) using 5-aminolevulinic acid (5-ALA) is now widely used in the neurosurgical resection of brain tumors since Stummer et al. revealed its advantage of increasing the resection ratio of the tumor [1–3]. The effect is that 5-ALA-induced protoporphyrin IX (PpIX) is accumulated in glioma cells and fluoresces at a 635 nm peak wavelength when irradiated at a 405 nm peak wavelength [4]. Kaneko et al. [5, 6] investigated the mechanism of fluorescence induced by 5-ALA and availability of fluorescence guided resection of malignant glioma. Panciani et al. [7] analyzed the advantages and limitations of fluorescence and image-guided resection. Diez Valle et al. [8] also analyzed the efficacy and applicability of surgery guided by 5-ALA fluorescence in consecutive patients with GBM. Roberts et al. [9] showed a significant relationship between the contrast enhancement on preoperative magnetic resonance imaging and observable intraoperative PpIX fluorescence. Hefti et al. [10, 11] reported the feasibility of the method in daily clinical practice and its technical limitations. Eljamel [12] reviewed comprehensively on Photodynamic applications in brain tumors. Stummer et al. [13] assessed the reliability of visible 5-ALA-induced fluorescence by spectrometry, pathology, and imaging.

There are many reports on the effectiveness of the fluorescence induced by 5-ALA for distinguishing the tumor part that requires resection and also when checking for any remaining tumor after the main part has been resected [14, 15, 16, 17]. However, it is difficult to precisely distinguish the margin of the tumor and infiltrating region when the fluorescence is vague. One of the efforts to solve this problem is silencing of ferrochelatase proposed by Teng et al. [18].

Confocal microscope has an advantage to observe in microscale with high resolution. There have been several attempts to apply confocal microscope for the resection of tumors. Sanai et al. [19] used a handheld confocal microscope in order to distinguish tumors in low grade gliomas. Eschbacher et al. [20] indicated that intraoperative confocal imaging was correlated with corresponding traditional histological findings. Martirosyan et al. [21] assessed the feasibility of handheld confocal endomicroscope imaging with various rapid fluorophores to provide histological information on gliomas, tumor margins, and normal brains in animal models. Mooney et al. [22] provided a comprehensive summary of laser scanning confocal endomicroscopy in animal and human neurosurgical studies. Liu et al. [23] reviewed the trends in fluorescence image-guided surgery for gliomas and Hadjipanayis et al. [24] reviewed the surgical benefit of utilizing 5-ALA for fluorescence-guided surgery of malignant gliomas. Although a confocal microscope has an advantage on viewing tumors at the microscale, it is not clear how infiltrating tumors appear in the confocal microscope view and whether the confocal microscope is useful for distinguishing the tumor in the boundary area.

We observed resected tumor areas following neurosurgery using a confocal microscope and investigated the data treatment method of confocal microscopic imaging [25]. To date, more than 20 samples have been inspected. In this report, fluorescence intensity analysis and a bright spot analysis are proposed for the precise distinction of brain tumors, and could be a useful surgical and photodynamic treatment modality.

2. Methods

2.1 Observation system using a confocal microscope

The observation system is shown in Fig. 1. We used a CSU22Z confocal laser-scanning microscope (Yokogawa Electric Corporation). A confocal microscope detects only the focused image that passes through a pinhole and presents a very clear image at the microscale. The chosen confocal microscope showed a good performance for taking pictures rapidly using multiple pinholes and microlenses in a rotating disk.

The imaging laser used was a 405 nm laser D405C-50 at 50 mW (Showa Optronics). A band pass filter from 610–680 nm wavelength was used in order to detect only the red fluorescence. The fluorescence was captured by the electron multiplying charge coupled device (EMCCD) camera ANDOR/LucaS658M. An objective lens 40×, PlanApo, NA 0.95, OLYMPUS/UPLSAPO40X2 was used. The observed area for one picture was 164.5 μm × 125 μm and the EMCCD camera produced pictures containing 658 × 496 pixels. Therefore, the observed area for one pixel was about 0.25 μm × 0.25 μm.

Precise positioning of the XY stage was used to construct a scanning picture map. The software iQ was used to move the stage and capture the image. For example, in order to achieve a map of 6.4 mm × 3.7 mm, 40 × 30 pictures must be obtained. Using this system, a fluorescence map composed of clear detailed images could be obtained in the normal surgery microscope scale. Such a wide view is necessary to compare with a hematoxylin and eosin (H&E) stained image and to find the same position for detailed comparisons at the microscale.

2.2 Specimens

Before surgery, a single administration of ALA at a dose of 20 mg/kg of body weight was given orally. ALA was dissolved in approximately 100 mL of juice and given to the patient approximately three hours before anesthesia. Resection was carried out following a standard microsurgical technique. Typically, the surgeon alternated between white and violet–blue light-emitting modes to visualize fluorescence during the resection. GBM specimens were collected at various times during the procedure in regions displaying both PpIX-positive and -negative visual fluorescence. For patients with deep-seated GBM underneath the cerebral cortex, GBM tissue was resected from areas with invasion area and normal brain. From the resected piece, a part of the red fluorescent region and surrounding non-fluorescent tissue and a boundary piece between the red fluorescent region and non-fluorescent region were both sent separately for pathological

and confocal microscope examinations.

Three serial sliced specimens of 10-μm thickness were cut from each piece. One slice of the specimen was observed as a H&E stain for a pathological inspection using a normal optical microscope. The second slice was observed by a confocal microscope and the third one was reserved.

A pathological inspection was made of the H&E image, and a comparison between the H&E and confocal microscope images at the same position was conducted. According to the pathological inspection, each area in the sliced part was evaluated as tumor region, infiltrating region and normal region. Although the sliced specimens were of different 10-μm thickness cross-sections, it was confirmed that nearly the same confocal microscope images were obtained from the slice before the H&E stain and the serial slice next to the H&E stain slice. Therefore, the confocal microscope image on one slice was compared with a serial slice H&E image.

2.3 Fluorescence intensity analysis

The fluorescence intensity of each pixel was obtained from a confocal microscope image. A histogram of the number of pixels having the same fluorescence intensity is provided in Fig. 2 and shows the districted area where a pathological inspection was made of the yielded tumor, infiltrating tumor, or normal tissue. It should be emphasized that x-axis does not mean wavelength but is the fluorescence intensity, and the y-axis represents the number of pixels that have the same fluorescence intensity. The average fluorescent intensity was also obtained from the districted area and all histograms were normally distributed.

A histogram of dark intensity that was captured without a sample is also displayed. The R value implies that the specimen intensity exceeded the dark intensity obtained from both fluorescent and dark histograms (Fig. 3). The reason why the dark intensity histogram was necessary is as follows. Each pixel on the EMCCD has dark noise and it is also detected at the same time. Because the dark noise of the pixel is not constant, even at the same temperature, it is impossible to substitute the dark intensity from the observed intensity to obtain the net fluorescent intensity on each pixel. Therefore, statistical techniques, such as the R value, were inspected.

2.4 Bright spot analysis

Image binarization was applied to the intensity of a pixel in the confocal microscope. A pixel with fluorescence larger than the 550 threshold value in this report was counted as a bright pixel. Pixels that connected with another bright pixel were counted as being in the same spot. The number of pixels included in one bright spot is referred to as the spot size. The number of bright spots in the image larger than the minimum spot size of 40 in this report is referred to as the bright spot number. A histogram of bright spot sizes is shown in Fig. 4. The x-axis refers to the bright spot size and the y-axis refers to the number of same spot sizes. The minimum spot size affects only the height of the first left side bar in the histogram and does not influence the skew of the histogram. The threshold value was located in the larger value area than the

average value of fluorescence intensity. Therefore, a bright spot analysis can be used to compare the distribution of fluorescence intensity in the region of high intensity between similar histograms of fluorescent intensity.

3. Results

3.1 Comparison between a confocal microscope image and pathological inspection of H&E

An example of the analysis obtained from one resected sample is presented. A tumor sample was taken from the red fluorescence area and a marginal sample was taken from the boundary area.

A comparison of the H&E stain and confocal microscope images are shown in Figs. 5 (a) and (b). Both of them were taken from the red fluorescence region. The confocal microscope image shows a part of the area from 40 × 30 pictures. The H&E image was made from images taken by an optical microscope at almost the same area as the confocal microscope image. The two districted confocal microscope and H&E images were then compared in detail (Fig. 5(c) and Fig. 5(d)). In Fig. 5(c), a pathological inspection of the H&E area [(1) in Fig. 5 (b)] shows a high density tumor. The corresponding confocal microscope image contains 4 × 5 pictures. A white backlight and some bright spots appear in the confocal microscope image. In Fig. 5(d), a pathological inspection of the H&E area [(2) in Fig. 5 (b)] shows a low-density tumor. The white fluorescence in the corresponding confocal microscope image looks weaker than in the area of (1).

The second specimen was taken from the boundary region [Fig. 6 (a) and (b)]. This specimen was divided into three areas of the tumor, infiltrating tumor, and normal tissue from a pathological view. The three districted areas, (3), (4), and (5) were compared as shown in (c), (d), and (e), respectively. A slightly larger bright spot appeared with no white background in the tumor region in the confocal microscope image [(c) (i)]. The confocal microscopy image of the infiltrating region has some similarities with the tumor region [(d) (i)]. The confocal microscopy image of the normal region contains many small bright spots [(e) (i)].

3.2 Investigation of fluorescence intensity

The distribution of pixel number with the same fluorescence is shown in Fig. 7. The peak distributions of the tumor (1) and (2) in Fig. 5 (a) are situated in higher intensities than other distributions. However, the distributions of the tumor in the boundary (3), infiltration region (4) and normal region (5) in Fig. 6(a) were very similar. A comparison of the average fluorescence intensity is shown in Fig. 7(b). The tumor regions (1) and (2) have larger average values than the other regions. However, the differences among regions (3), (4), and (5) were all small. The R values (Fig. 7(c)) show an enhanced difference between the tumor regions (1) and (2) and other regions. The differences among (3), (4), and (5) remain small.

3.3 Bright spot analysis

Histograms of the bright spot numbers with same spot size are made on regions (3), (4), and (5), shown as Figs. 8 (a), (b), and (c), respectively. Large differences appeared between the tumor region (3) or the infiltrating region (4) and the normal region (5), and there were some large-sized spots in (3) and (4). On the other hand, there were a large number of small spots in the normal region (5). The average bright spot size and total number of spots are compared in (d) (i) and (ii). The average spot size was large in regions (3) and (4) and small in the normal region (5). The total spot number was lower in (3) and (4) and higher in the normal region (5). Therefore, the difference between an infiltrating tumor region and the normal region appears clearly in comparisons of spot number and size.

Results on average fluorescence intensity, R value, number of bright spots and average bright spot size are summarized in Table 1.

4. Discussion

4.1 Distinction of the tumor from the normal region

In the bright area of the red fluorescence, the fluorescence occurs over the entire area. This means that PpIX was diffused not only inside the cell, but also outside the cell. The average fluorescence was larger than that in the normal region and distinguishing a tumor was easy. The value of the average fluorescence of the tumor region differs by each sample case. However, the value that appeared in the visibly red area was almost apparently a larger value than that in the normal region.

The R values demonstrated the differences between the tumor and normal regions. However, in the case of the marginal zone or infiltrating area, the difference of the pixel fluorescence distribution, average intensity, and R values became small compared with normal values.

Hefti et al. [10] detected fluorescence intensity using a photomultiplier and made a virtual fluorescence intensity map on a heads-up display. This was of enormous help to surgeons. Our investigation using confocal microscopy offers a more detailed evaluation on a microscopic scale. In the present study, fluorescence intensity was obtained in the area of 0.64 mm × 0.6 mm; for this area, 4 images × 5 images = 20 images were taken by the confocal microscope. The intensity value can be obtained from each image measuring 0.164 mm × 0.128 mm and also from a wider area than that shown in the present study. The fluorescence intensity map is also obtained from each demarcated area on the scan-detected figures. However, with the use of only this method, the precise boundary between the infiltrating region and normal region cannot be obtained in cases wherein the infiltrating region has low fluorescence. Therefore, another investigative method is necessary to distinguish normal from infiltrating tissue. One possible solution is the analysis of the bright spot size and number proposed in the present study.

Ejamel et al. [26] found that the mean diameter of new GBM induced by 5-ALA fluorescence was wider than that demonstrated by enhanced MRI. This shows the usefulness of the 5-ALA fluorescence method for examining the precise resection area. Our technique using confocal microscopy is able to make a more detailed evaluation of the tumor boundary under fluorescence induced by 5-ALA.

4.2 Distinction of infiltrating tumor from the normal region

Although the average fluorescence was not different between the marginal and infiltrating zones and the normal region, the bright spot size and the total number of spots were different between them. Therefore, there is a possibility to discriminate between the infiltrating tumor zones from the normal region using the inspection of bright spot sizes and numbers. Of course, the comparison of bright spot size and number reported here is only one example in a clinical neurosurgery setting. The application of this inspection method must be investigated in many diverse cases of brain tumor resection surgery.

Sanai et al. [19] made important challenges to intraoperative confocal microscopy using a handheld single-fiber scanning technique in the visualization of fluorescence induced by 5-ALA in low-grade gliomas. They found multiple fluorescent spots in the tumor and tumor margins and no bright spots in radiographically tumor-free areas. This indicates that visualization using confocal microscopy is useful in investigating even low fluorescence areas to delineate tumor margins. However, they did not investigate how fluorescence spots appear in marginal areas of high- and low-grade gliomas. Using the confocal microscope, we observed normal regions and evaluated them by histological inspection of H&E stained images which showed fluorescent spots in every resected section of the specimen; in the tumor area, the fluorescence appeared like a cloud covering the entire area. There must be some transient status from small bright spots distributed in the normal areas to the cloudy fluorescence of the tumor region in the infiltrating region. The analysis of the spot size and number remains a challenge in investigating the transient status of the infiltrating region and marginal region.

4.3 Availability for *in vivo* diagnosis in neurosurgery

Once the reliability of a diagnosis using fluorescence inspection and bright spot analysis at the microscale is established, an *in vivo* diagnosis of 5-ALA-induced PDD in neurosurgery can be applied to either a microscope or confocal microscope technique during neurosurgery. It is important to be able to confirm the position in the view of a microscope for a successful tumor removal. Because the area of observation by a confocal microscope is very small, a combination of the neurosurgery microscope and the confocal microscope is necessary for the accurate determination of infiltrated areas.

Moreover, its combination with Photo Dynamic Therapy (PDT) will be useful if the distinguished area by PDD is directly lighted by the laser of PDT.

5. Conclusions

The methods of fluorescence intensity analysis and bright spot analysis have been proposed using a confocal microscope for the precise discrimination of a brain tumor by 5-ALA PDD. The discrimination of a tumor region from a normal region by a fluorescence intensity analysis is very useful. An analysis of the bright spot size and the total spot number will be useful to discriminate between the infiltrating tumor and normal regions. The authors hope that the reliability of these diagnoses methods will be established in various neurosurgery cases and the methods will facilitate the precise resection or precise PDT of brain tumor tissue.

Acknowledgements

The authors thank Takuma Katahira and Yusuke Ito, who were master course students in Kanazawa University, for their cooperation in the progress of this research. The authors also thank Hemuragul Sabit for help with the pathological inspection of the resected specimens. The authors wish to appreciate the technical staffs in Yokogawa Electric Corporation for their technical assistance in the operation technology of the confocal microscope.

Funding

This research was supported by JSPS KAKENHI Grant Number 26242054.

Compliance with ethical standards

Conflict of interest

The authors declare that they have no conflict of interest.

Ethical approval

This study has been permitted by the ethical committee of Kanazawa University as No. 209-7.

Informed consent

Informed consent was obtained from all individual participants included in the study.

References

1. W. Stummer, S. Stocker, S. Wagner, H. Stepp, C. Fritsch, C. Goetz, AE. Goetz, R. Kiefmann, HJ. Reulen, Intraoperative detection of malignant gliomas by 5-aminolevulinic acid-induced porphyrin fluorescence, Neurosurgery 42: (1998) 518-526.
2. W. Stummer, A. Novotny, H. Stepp, C. Goetz, K. Bise, HJ. Reulen, Fluorescence-guided resection of

glioblastoma multiforme by using 5-aminolevulinic acid—induced porphyrins: a prospective study in 52 consecutive patients, J Neurosurgery 93: (2000) 1003-1013.

3. W. Stummer, U. Pichlmeier, T. Meinel, OD. Wiestler, F. Zanella, HJ. Reulen, Fluorescence-guided surgery with 5-aminolevulinic acid for resection of malignant glioma:randomized controlled multicenter phase Ⅲ trial, Lancet Oncol 7: (2006) 392-401.
4. W. Stummer, S. Stocker, A. Novotny, A. Heimann, O. Sauer, O. Kempski, N. Pressnilla, J. Wietzorrek, HJ. Reulen, In vitro and in vivo porphyrin accumulation by C6 glioma cells after exposure to 5-aminolevulinic acid, J Photochem Photobiol B 45: (1998) 160-169.
5. S. Kaneko, I.Okura, T.Tanaka, Photodynamic applications (PDD, PDT) using aminolevulinic acid in neurosurgery, Aminolevulinic Acid, SBI ALApromo: (2015) 119-140.
6. S. Kaneko, S. Kaneko, Fluorescence-Guided Resection of Malignant Glioma with 5-ALA, International Journal of Biomedical Imaging, Volume 2016: (2016) 1-11.
7. PP. Panciani, M. Fontanella, B. Schatlo, D. Garbossa, A. Agnoletti, A. Ducat, M. Lanotte M, Fluorescence and image guided resection in high grade glioma, Clin Neurol Neurosurg114(1): (2012) 37-41.
8. R. Diez Valle, S. Tejada Solis, MA. Idoate Gastearena, R. Garcia de Eulate, P. Dominguez Echavarri, J. Aristu Mendiroz, Surgery guided by 5-aminolevulinic fluorescence in glioblastoma: volumetric analysis of extent of resection in single-center experience, J Neurooncol 102: (2011) 105-113.
9. DW. Roberts, PA. Valdes, BT. Harris, KM. Fontaine, A. Hartov, X. Fan, S. Ji, SS. Lollis, BW. Pogue, F. Leblond, TD. Tosteson, BC. Wilson, K. Paulsen, Coregistered fluorescence-enhanced tumor resection of malignant glioma: relationship between δ-aminolevulinic acid-induced protoporphyrin Ⅸ fluorescence, magnetic resonance imaging enhancement, and neuropathological parameters. Clinical article, J Neurosurg 114: (2011) 595-603.
10. M. Hefti, G. von Campe, M. Moschopulos, A. Siegner, H. Looser, H. Landolt, 5-aminolevulinic acid induced protoporphyrin Ⅸ fluorescence in high-grade glioma surgery: a one-year experience at a single institution, Swiss Med Wky 138: (2008) 180-185.
11. M. Hefti, H. M. Mehdorn, I. Albert, L. Dörner, Fluorescence-Guided Surgery for Malignant Glioma: A Review on Aminolevulinic Acid Induced Protoporphyrin IX Photodynamic Diagnostic in Brain Tumors, Current Medical Imaging Reviews, 2010, Vol.6, No.4 :(2010) 1-5.
12. S.Eljamel, Photodynamic applications in brain tumors: A comprehensive review of the literature, Photodiagnosis and Photodynamic Therapy (2010) 7, 76-85.
13. W. Stummer, JC. Tonn, C. Goetz, W. Ullrich, H. Stepp, A. Bink, T. Pietsch, U. Pichlmeier, 5-aminolevulinic acid-derived tumor fluorescence: the diagnostic accuracy of visible fluorescence qualities as corroborated by spectrometry and histology and postoperative imaging, Neurosurgery 74: (2014) 310-319.
14. S. Utsuki, H. Oka, S. Sato, S. Suzuki, S. Shimizu, S. Tanaka, K. Fujii, Possibility of using laser

spectroscopy for the intraoperative detection of nonfluorescing brain tumors and the boundaries of brain tumor infiltrates, Technical note, J Neurosurgery 104: (2006) 618-620.

15. K. Roessler, A. Becherer, M. Donat, M. Cejna, I. Zachenhofer, Intraoperative tissue fluorescence using 5-aminolevulinic acid (5-ALA) is more sensitive than contrast MRI or amino acid positron emission tomography ((18)F-FET PET) in glioblastoma surgery, Neurol Res 34: (2012) 314-317.
16. G. Widhalm, B. Kiesel, A. Woehrer, T. Traub-Weidinger, M. Preusser, C. Marosi, D. Prayer, JA. Hainfellner, E. Knosp, S. Wolfsberger, 5-Aminolevulinic acid induced fluorescence is a powerful intraoperative marker for precise histopathological grading of gliomas with non-significant contrast-enhancement, Plos One 8: (2013) e76988.
17. G. Widhalm, S. Wolfsberger, G. Minchev, A. Woehrer, M. Krssak, T. Czech, D. Prayer, S. Asenbaum, JA. Hainfellner, E. Knosp, 5-Aminolevulinic acid is a promising marker for detection of anaplastic foci in diffusely infiltrating gliomas with nonsignificant contrast enhancement, Cancer 116: (2010) 1545-1552.
18. L. Teng, M. Nakada, S-G. Zhao, Y. Endo, N. Furuyama, E. Nambu, IV. Pyko, Y. Hayashi, JI. Hamada, Silencing of ferrochelatase enhances 5-aminolevulinic acid-based fluorescence and photodynamic therapy efficacy, Br J Cancer 104: (2011) 798-807.19. N. Sanai, LA. Snyder, NJ. Honea, SW. Coons, JM. Eschbacher, KA. Smith, RF. Spetzler, Intraoperative confocal microscopy in the visualization of 5-aminolevulinic acid fluorescence in low-grade gliomas, J Neurosurg 115: (2011) 740-748.
20. J. Eschbacher, NL. Martirosyan, P. Nakaji, N. Sanai, MC. Preul, KA. Smith, SW. Coons, RF. Spetzler, In vivo intrraperative confocal microscopy for real-time histopathological imaging of brain tumors, J Neurosurg 116: (2012) 854-860.
21. NL. Martirosyan, J. Georges, JM. Eschbacher, DD. Cavalcanti, AM. Elhadi, MG. Abdelwahab, AC. Scheck, P. Nakaji, RF. Spetzler, MC. Peul, Potential application of a handheld confocal endomicroscope imaging system using a variety of fluorophores in experimental gliomas and normal brain, Neurosurg Focus 36: (2014) 1-14.
22. MA. Mooney, AH. Zehri, JF. Georges, P. Nakaji, Laser scanning confocal microscopy in the neurosurgical operating room: a review and discussion of future applications, Neurosurg Focus 36(2): (2014).
23. J. Liu, D. Meza, N. Sanai, Trends in fluorescence image-guided surgery for gliomas, Neurosurgery 75: (2014) 61-71.
24. CG. Hadjipanayis, G. Widhalm, W. Stummer, What is the surgical benefit of utilizing 5-aminolevulinic acid for fluorescence-guided surgery of malignant gliomas? Neurosurgery 77: (2015) 663-673.
25. K. Togano, T. Yoneyama, J. Hamada, Y. Hayashi, M. Nakada, T. Watanabe, H. Kagawa, Observation of brain tumor for the discrimination using a confocal laser scanning microscope, Transaction of the Japanese Society for Medical and Biological Engineering,50: (2012) 62-67.
26. S. Eljamel, M. Petersen, R. Valentine, R. Buist, C. Goodman, H. Moseley, S. Eljamel, Comparison of

intraoperative fluorescence and MRI image guided neuronavigation in malignant brain tumors, a prospective controlled study, Photodiagnosis and Photodynamic Therapy (2013) 10, 356-3

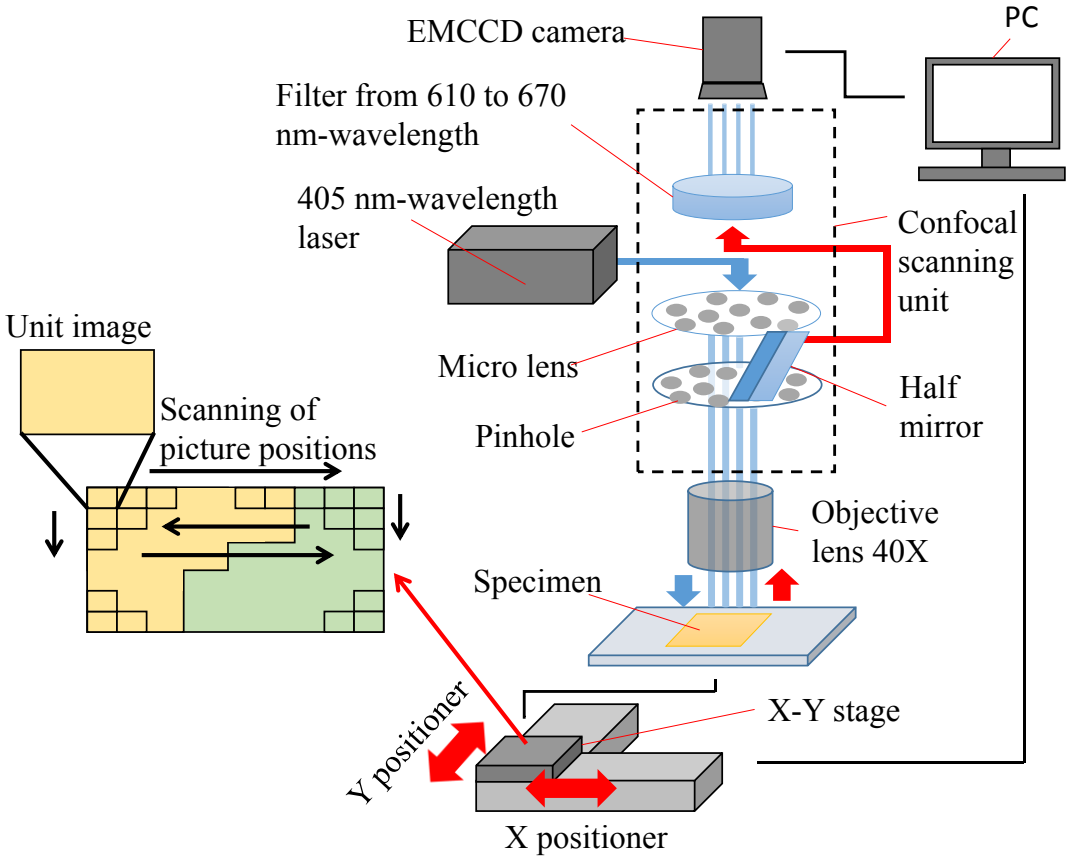

Fig. 1 Confocal microscope system

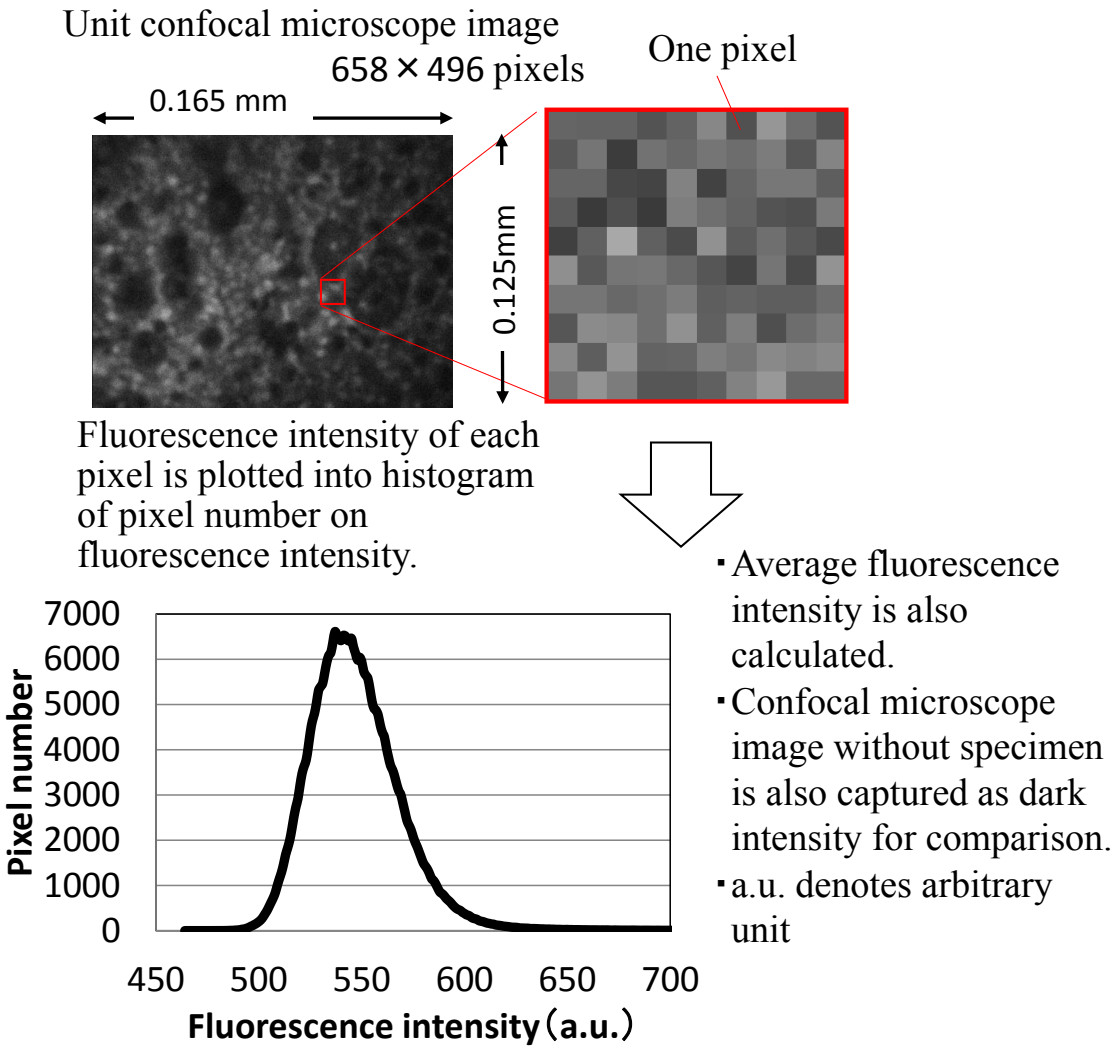

Fig.2 Fluorescence intensity analysis from the captured image

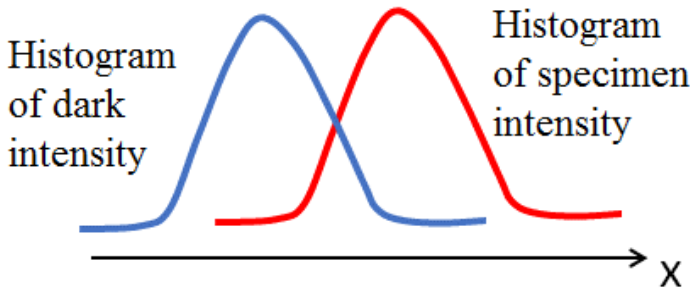

$$P_f' = \emptyset\left(-\frac{\mu_t - \mu_d}{\sqrt{\sigma_t^2 + \sigma_d^2}}\right) = 1 - \emptyset\left(\frac{\mu_t - \mu_d}{\sqrt{\sigma_t^2 + \sigma_d^2}}\right)$$

μ_t : Average of specimen intensity
σ_t : Standard deviation of specimen intensity
μ_d : Average of dark intensity
σ_d : Standard deviation of dark intensity
Φ : Probability density function of standard normal distribution
P'_f: Probability that the intensity in the dark image exceeds that in the specimen
R: Probability that the intensity in the specimen exceeds that in the dark image

$$R = 1 - P'_f$$

Fig.3 Probability that the intensity of the specimen exceeds that of the dark image

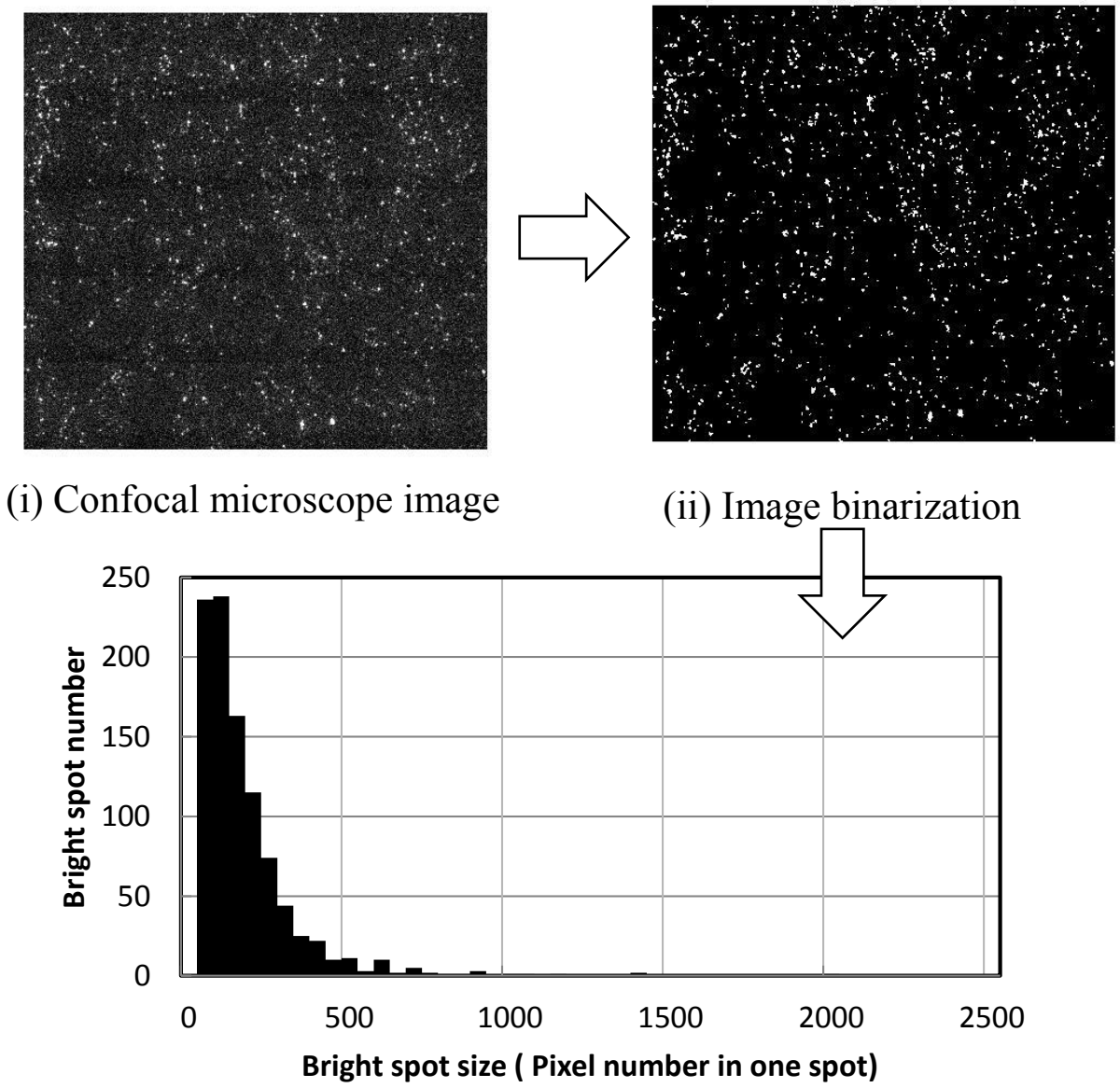

Fig.4 Bright spot size and spot number analysis

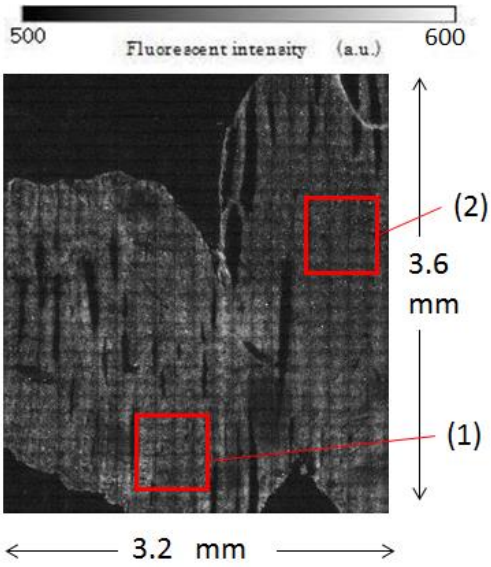

(a) Confocal microscopy fluorescence image

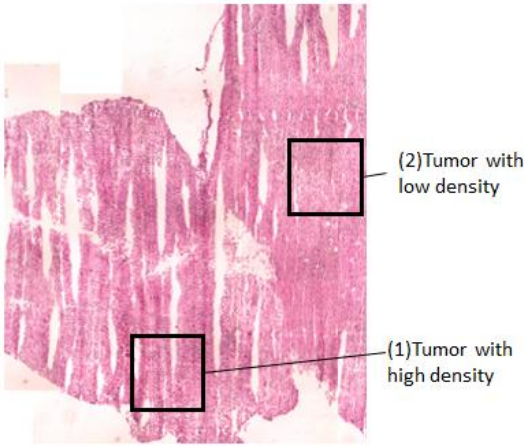

(b) H&E image and pathological inspection

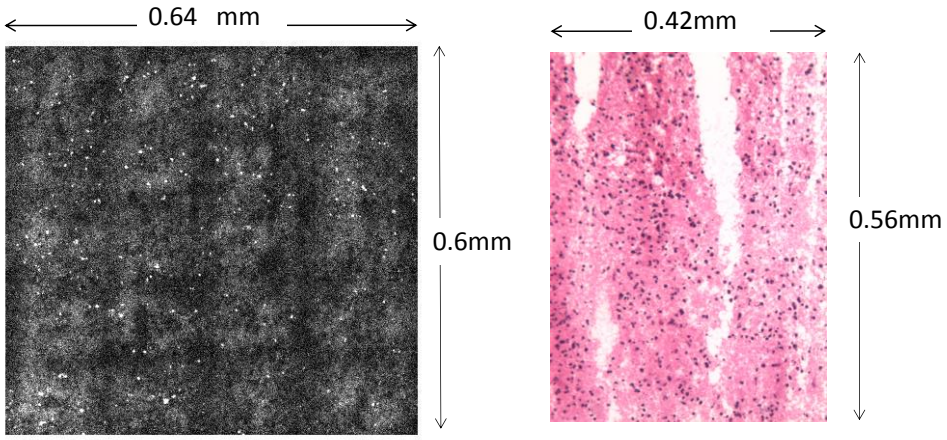

(i) Confocal microscopy image (ii) H&E image

(c) Comparison between confocal microscopy image and H&E image at (1) tumor with high density

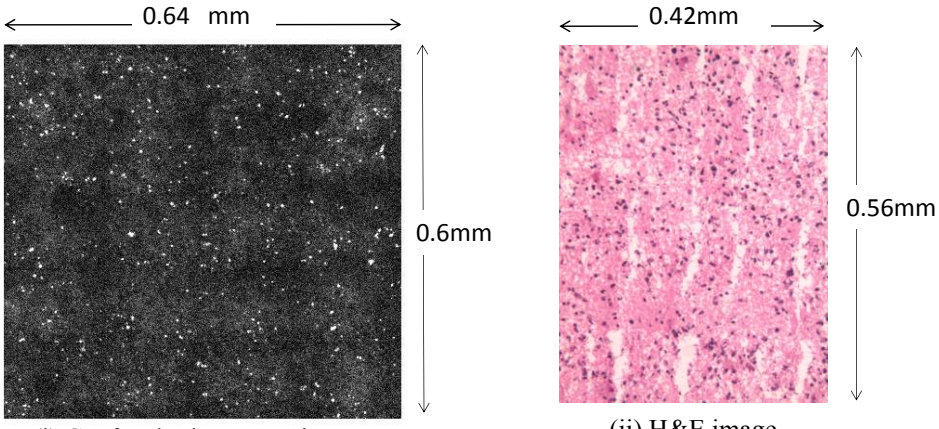

(i) Confocal microscopy image (ii) H&E image

(d) Comparison between confocal microscopy image and H&E image at (2) tumor with low density

Fig.5 Comparison between confocal image and H&E image on the specimen from tumor area

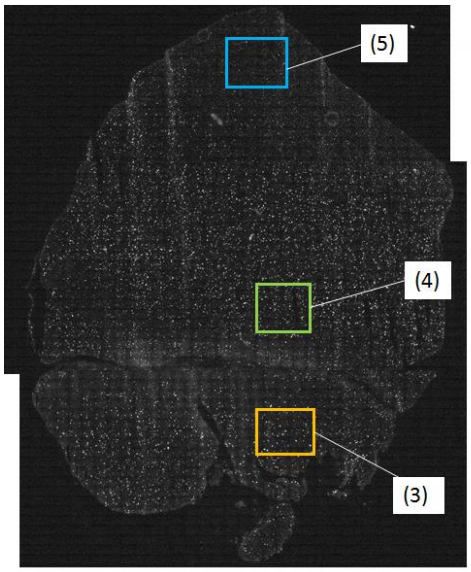

(a)Confocal microscopy fluorescence image

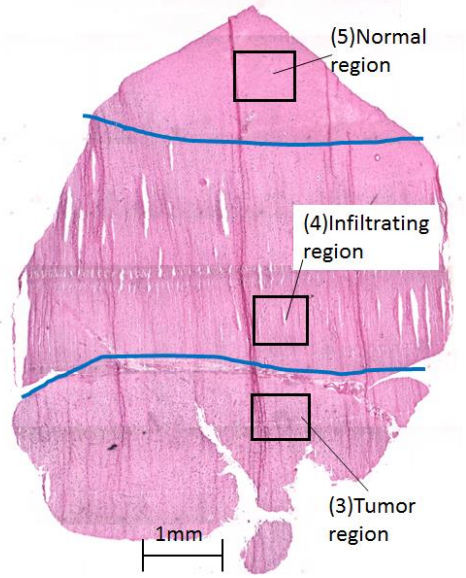

(b) H&E image and pathological inspection

(c) Comparison between a confocal image and an H&E image at (3) tumor in the boundary

(d) Comparison between a confocal image and an H&E image at (4) infiltrating tumor area

(e) Comparison between a confocal image and an H&E image at (5) normal area

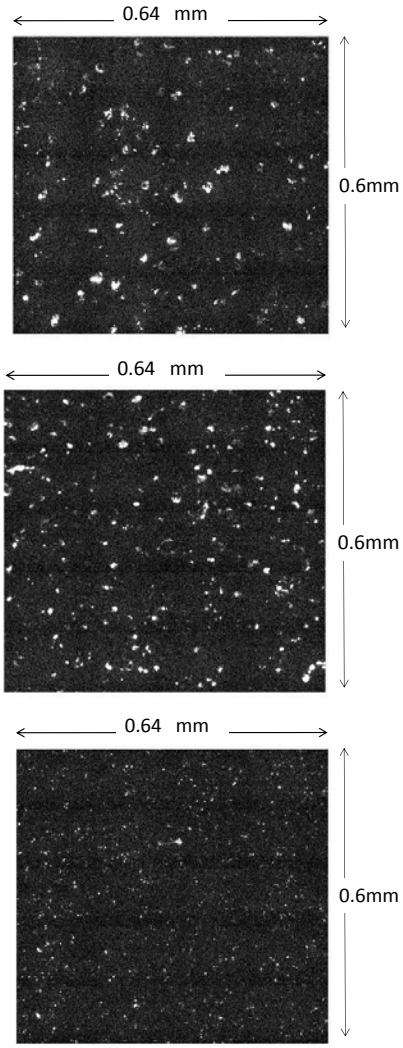

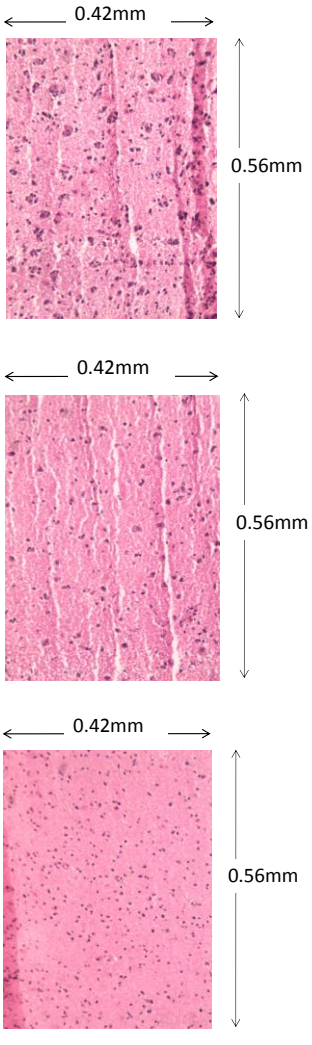

(i) Confocal microscopy image

(ii) H&E image

Fig. 6 Comparison between confocal microscopy image and H&E image on the specimen from boundary area

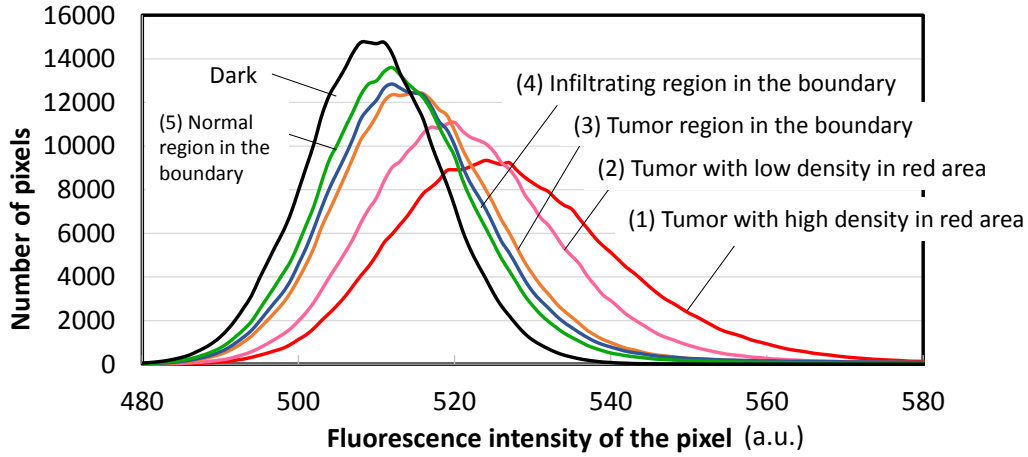

(a) Histogram of pixels with specific fluorescence intensity

Fig.12 Histogram of pixels on fluorescence intensity

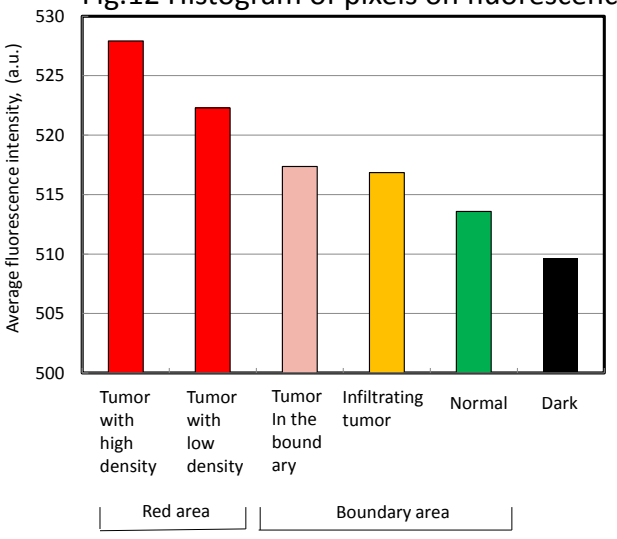

(b) Comparison of the average fluorescence intensity

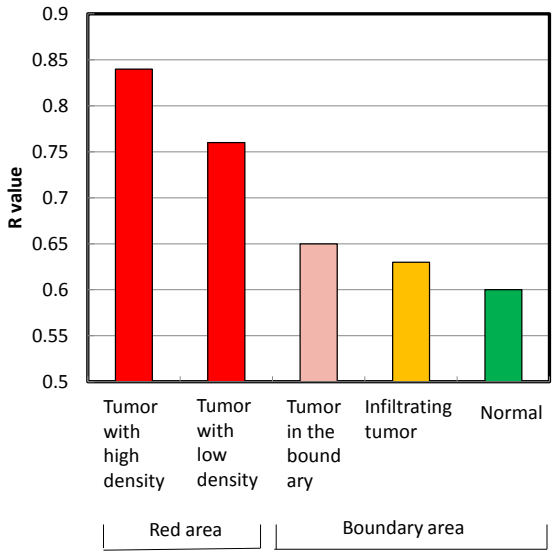

(c) Comparison of the R value, which implies that the probability of not being in the dark distribution

Fig. 7 Fluorescence intensity analysis

(a) Histogram of the bright spot number in a spot size in the (3) tumor at the boundary

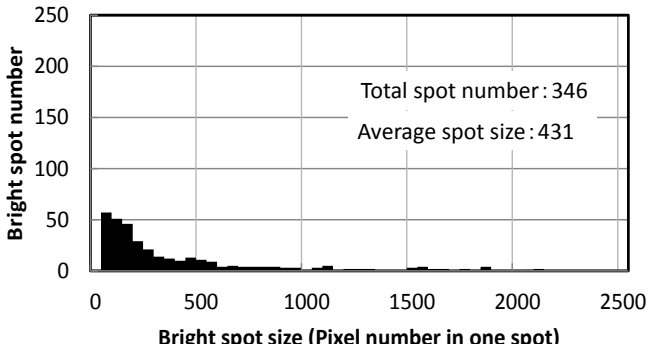

(b) Histogram of the bright spot number in a spot size in the (4) infiltrating tumor

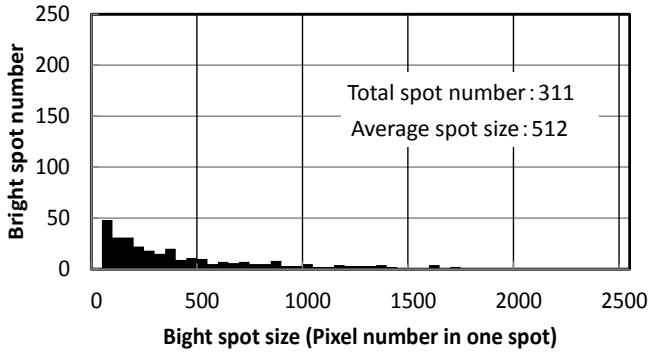

(c) Histogram of the bright spot number in a spot size in the (5) normal area

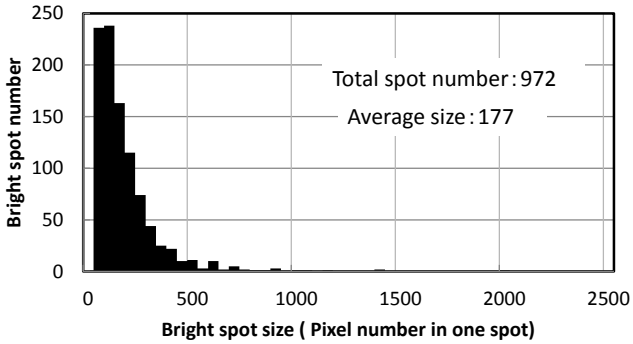

(d) Comparison of average spot sizes and number of spots

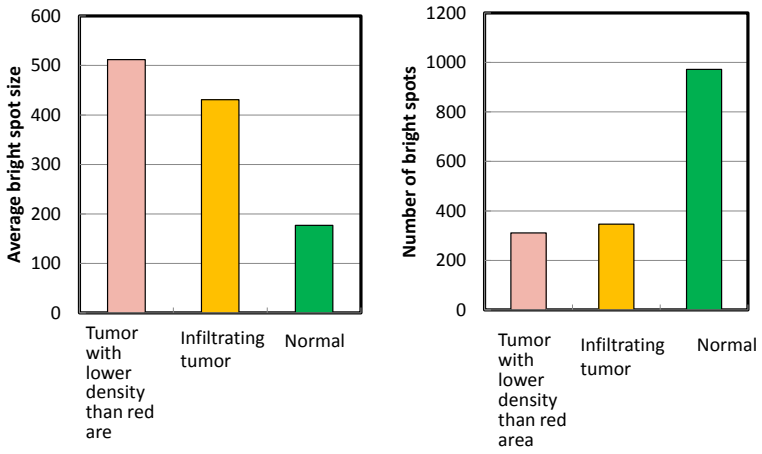

(i) Average bright spot size (ii) Number of the spots

Fig.8 Spot size analysis on the specimen from boundary area

Legends of figures

Fig.1 Confocal microscope system

Fig.2 Fluorescence intensity analysis from the captured image

Fig.3 Probability that the intensity of the specimen exceeds that of the dark image

Fig.4 Bright spot size and spot number analysis

Fig.5 Comparison between confocal microscopy image and H&E image on the specimen from tumor area

Fig.6 Comparison between confocal microscopy image and H&E image on the specimen from boundary area

Fig.7 Fluorescence intensity analysis

Fig.8 Spot size analysis on the specimen from boundary area

Table 1　Results on fluorescence intensity and bright spot analysis

	Region No.	Pathological inspection	Average fluorescence intensity	R value	Number of bright spots	Average bright spot size
Sample from red fluorescent area	(1)	Tumor with high density	527.92	0.84		
	(2)	Tumor with low density	522.28	0.76		
Sample from boundary area	(3)	Tumor region	517.37	0.65	311	512
	(4)	Infiltrating region	516.85	0.63	346	431
	(5)	Normal region	513.58	0.60	972	177
No specimen		Dark	509.64	0.5		